

## CHAPTER 8

# *Manipulating Singlet Order by Spin-lock Induced Crossing*

STEPHEN J. DEVIENCE<sup>a</sup> AND MATTHEW S. ROSEN<sup>\*b,c,d</sup>

<sup>a</sup>West Virginia University School of Medicine, Department of Biochemistry, 64 Medical Center Drive, Morgantown, WV 26506, USA; <sup>b</sup>A. A. Martinos Center for Biomedical Engineering, Massachusetts General Hospital, 149 13th Street, Suite 2301, Charlestown, MA 02129, USA; <sup>c</sup>Harvard Medical School, Boston, MA, USA; <sup>d</sup>Harvard University, Department of Physics, Cambridge, MA, USA

\*Email: rosenm@nmr.mgh.harvard.edu

## 8.1 Introduction

Singlet states created in strongly coupled spin systems can exhibit long lifetimes without the need for sustaining pulses, which makes them attractive for applications such as MRI where high RF power needs to be avoided. However, in the strong coupling regime, conventional pulse sequences are unable to create singlet order from triplet magnetization. Previously, the M2S sequence was introduced, which can perform this task *via* a sequence of hard pulses. This chapter discusses an alternative family of methods for singlet order creation and manipulation, called spin-lock induced crossing (SLIC), which instead utilizes weak spin-locking pulses.

Spin-locking is the application of a long RF pulse or pulse train designed to hold magnetization along a projection in the transverse plane. In its simplest form, CW spin-locking, a single RF pulse is applied on resonance with the spins with  $B_1$ , the induced magnetic field in the rotating frame, along the same direction as the spin magnetization.<sup>1</sup> This differs from a

typical NMR pulse, in which  $B_1$  is applied perpendicular to the axis of magnetization in order to rotate it from one axis to another. Spin-locking instead creates an energy splitting in the rotating frame, proportional to the magnitude of  $B_1$ , which suppresses relaxation due to inhomogeneities and slow  $B_0$  fluctuations. The transverse magnetization lifetime during spin-locking is then described by a constant  $T_{1\rho}$ .

For a system of coupled spins, spin-locking not only creates an energy splitting but also changes the symmetry of the spin eigenstates.<sup>2</sup> This is clear from previous chapters, where spin-locking was shown to convert coherences between Zeeman states to population differences between singlet and triplet states, which have entirely different relaxation properties. Therefore, in the presence of spin-locking fields, it is most appropriate to work in the “dressed states” basis, which results from diagonalization of the Hamiltonian with the spin-locking terms included. From this Hamiltonian, and in the presence of molecular couplings, a variety of rich behaviors arise that can be controlled by the three selectable spin-locking parameters: resonance frequency  $\nu_0$ , nutation frequency  $\nu_n$  (also called Rabi frequency, which is proportional to  $B_1$  magnitude), and phase (aligned or anti-aligned with magnetization).

By selecting the appropriate parameters, SLIC can induce the creation of singlet order from triplet magnetization (and *vice versa*) or the transfer of singlet order between different groups of spins. The former enables spectroscopy of  $J$ -coupling and chemical shifts among strongly coupled spins<sup>3</sup> as well as the storage of magnetization as long-lived singlet order, which is useful for measuring slow diffusion<sup>4</sup> or preserving hyperpolarization beyond  $T_1$ .<sup>5–10</sup> The latter is useful for transferring polarization to long-lived singlet states following para-hydrogen induced polarization<sup>11–22</sup> and for measuring weak  $J$ -coupling differences in complex molecules.<sup>2,3</sup>

The following sections will describe the theory and applications of SLIC, beginning with a simple two-spin system and then moving on to more complicated cases.

## 8.2 The Two-spin System

The simplest system in which singlet and triplet states arise is in a pair of spin-1/2 nuclei interacting *via* scalar coupling, which is described by the Hamiltonian

$$\hat{\mathcal{H}} = -\nu_1 \hat{I}_{1z} - \nu_2 \hat{I}_{2z} + J_{12} \hat{I}_1 \cdot \hat{I}_2, \quad (8.1)$$

where units of Hz have been chosen for resonance frequencies  $\nu$  and scalar coupling  $J$ . The corresponding Zeeman eigenstates can be represented as  $|\uparrow\uparrow\rangle$ ,  $|\downarrow\downarrow\rangle$ ,  $|\uparrow\downarrow\rangle$ , and  $|\downarrow\uparrow\rangle$ . This case is common for pairs of protons,  $^{13}\text{C}$ , or  $^{15}\text{N}$  nuclei in liquid or gas state molecules, where dipolar coupling can be ignored (as it is averaged out by molecular tumbling and only contributes to spin relaxation). If the two spins have identical resonance frequencies,

$\Delta v = v_A - v_B = 0$ , diagonalization of the Hamiltonian reveals that the system is described by three symmetric triplet eigenstates and one anti-symmetric singlet state.<sup>24,25</sup> In terms of the Zeeman states, these are defined as

$$|T_+\rangle = |\uparrow\uparrow\rangle, \quad |T_0\rangle = (|\uparrow\downarrow\rangle + |\downarrow\uparrow\rangle)/\sqrt{2}, \quad |T_-\rangle = |\downarrow\downarrow\rangle, \quad |S_0\rangle = (|\uparrow\downarrow\rangle - |\downarrow\uparrow\rangle)/\sqrt{2}. \quad (8.2)$$

If the spins are not equivalent but the coupling is strong ( $J_{AB} \gg \Delta v$ ), it is also acceptable to make the approximation that these are the eigenstates, just as Zeeman eigenstates are generally used for the case of weakly coupled spins ( $J_{AB} \ll \Delta v$ ).

In matrix form, the Hamiltonian for the system with two identical spins in the basis (8.2) is

$$\hat{\mathcal{H}}_0 = \begin{bmatrix} -\frac{v_1 + v_2}{2} + \frac{J}{4} & 0 & 0 & 0 \\ 0 & \frac{J}{4} & 0 & 0 \\ 0 & 0 & \frac{v_1 + v_2}{2} + \frac{J}{4} & 0 \\ 0 & 0 & 0 & -\frac{3J}{4} \end{bmatrix}. \quad (8.3)$$

By working in the rotating frame, so that  $v_1 + v_2 = 0$ , the diagonal elements are simplified further, and triplet states become degenerate. When spin-locking is applied with nutation frequency  $v_n$ , it appears in the Hamiltonian as off-diagonal elements connecting the triplet states:

$$\hat{\mathcal{H}}_{SL} = \begin{bmatrix} \frac{J}{4} & \frac{v_n}{\sqrt{2}} & 0 & 0 \\ \frac{v_n}{\sqrt{2}} & \frac{J}{4} & \frac{v_n}{\sqrt{2}} & 0 \\ 0 & \frac{v_n}{\sqrt{2}} & \frac{J}{4} & 0 \\ 0 & 0 & 0 & -\frac{3J}{4} \end{bmatrix}. \quad (8.4)$$

Diagonalization into dressed states gives

$$\hat{\mathcal{H}}_{SL, \text{dressed}} = \begin{bmatrix} \frac{J}{4} - v_n & 0 & 0 & 0 \\ 0 & \frac{J}{4} & 0 & 0 \\ 0 & 0 & \frac{J}{4} + v_n & 0 \\ 0 & 0 & 0 & -\frac{3J}{4} \end{bmatrix}, \quad (8.5)$$

with new eigenstates

$$\begin{aligned}
 |\phi_+\rangle &= \frac{1}{2}(|\uparrow\uparrow\rangle + |\downarrow\downarrow\rangle - |\uparrow\downarrow\rangle - |\downarrow\uparrow\rangle) \\
 |\phi_0\rangle &= \frac{1}{\sqrt{2}}(|\downarrow\downarrow\rangle - |\uparrow\uparrow\rangle) \\
 |\phi_-\rangle &= \frac{1}{2}(|\uparrow\uparrow\rangle + |\downarrow\downarrow\rangle + |\uparrow\downarrow\rangle + |\downarrow\uparrow\rangle) \\
 |S_0\rangle &= \frac{1}{\sqrt{2}}(|\uparrow\downarrow\rangle - |\downarrow\uparrow\rangle).
 \end{aligned} \tag{8.6}$$

Note that these four eigenstates also arise from a weakly coupled spin pair if strong spin-locking is applied<sup>2</sup> (with  $v_n > 5\Delta v$ ). The singlet state symmetry and energy are unaffected by spin-locking, whereas the triplet states are rotated to match the new quantization axis along the spin-locking direction, *i.e.*, the states  $|\phi_-\rangle$ ,  $|\phi_0\rangle$  and  $|\phi_+\rangle$  are the triplet states  $|T_-\rangle$ ,  $|T_0\rangle$  and  $|T_+\rangle$  in the tilted frame with the quantization axis parallel to the  $x$ -axis. Moreover, the triplet states are no longer degenerate, and two of them now have energy levels that are linearly dependent on the spin-locking nutation frequency.

Eqn (8.5) shows that if a nutation frequency is applied with  $v_n = J$  or  $v_n = -J$ , the energy levels of eigenstates  $|\phi_+\rangle$  or  $|\phi_-\rangle$ , respectively, become equal to the energy of  $|S_0\rangle$ . We refer to this point as a spin-lock induced crossing<sup>3</sup> (SLIC). Here, any small interaction terms connecting the two crossing states can drive a coherent population transfer between them. If the spins are not exactly equivalent, there is in fact such a term arising from  $\Delta v$ , the resonance frequency difference between the two spins. Adding this term to the Hamiltonian gives

$$\hat{\mathcal{H}}_{SL, \text{dressed}} = \begin{bmatrix} \frac{J}{4} - v_n & 0 & 0 & \frac{\Delta v}{2\sqrt{2}} \\ 0 & \frac{J}{4} & 0 & 0 \\ 0 & 0 & \frac{J}{4} + v_n & -\frac{\Delta v}{2\sqrt{2}} \\ \frac{\Delta v}{2\sqrt{2}} & 0 & -\frac{\Delta v}{2\sqrt{2}} & -\frac{3J}{4} \end{bmatrix}. \tag{8.7}$$

When the system is held at the crossing point, there is an oscillation between the triplet and singlet state population with a period of  $\sqrt{2}\Delta v$ .

A SLIC sequence can therefore be used as an alternative to the M2S sequence<sup>26,27</sup> for preparing singlet order from triplet state magnetization, with a simple spin-locking pulse replacing the two pulse trains (Figure 8.1). As in M2S, the SLIC sequence begins with a  $90^\circ$  pulse to place magnetization into the transverse plane along  $x$ . With spin-locking off, the system is in a coherence  $(|T_-\rangle + |T_+\rangle)\langle T_0| + |T_0\rangle(\langle T_-| + \langle T_+|)$ , which then becomes a population difference  $|\phi_+\rangle\langle\phi_+| - |\phi_-\rangle\langle\phi_-|$  when spin-locking is applied. Maximum transfer to singlet is achieved after spin-locking with  $v_n = J$  for time  $1/(\Delta v\sqrt{2})$ , giving the

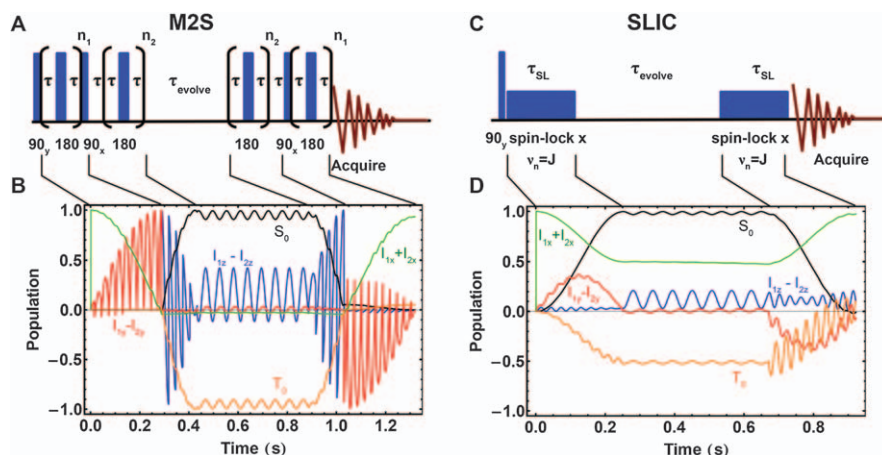


**Figure 8.1** Pulse sequences and simulated dynamics for singlet creation, evolution and readout using the M2S and SLIC pulse sequences. (a and b) Schematic and simulation of M2S experiment: Two series of pulse trains convert transverse magnetization first to a coherence and then to singlet order. Following evolution, the sequence is applied in reverse order to move magnetization back to the transverse plane for readout. (c and d) Schematic and simulation of SLIC experiment: A low-power spin-locking pulse directly transfers magnetization from the transverse plane to singlet order. Following evolution, the same spin-locking pulse returns the remaining magnetization to the transverse plane for readout. Reproduced from ref. 3 with permission from American Physical Society, Copyright 2013.

population difference  $|S_0\rangle\langle S_0| - |\phi_-\rangle\langle\phi_-|$  (or  $|\phi_+\rangle\langle\phi_+| - |S_0\rangle\langle S_0|$  if  $\nu_n = -J$ ). Half the  $x$ -axis magnetization has been depleted, which can be measured as a decrease in intensity if a spectrum is acquired at this point. Alternatively, after some time an identical spin-locking pulse can be applied to transfer remaining singlet order back to the  $x$ -axis for readout.

There are some interesting properties of eqn (8.7). First, whether  $|\phi_+\rangle\langle\phi_+|$  or  $|\phi_-\rangle\langle\phi_-|$  is converted to singlet population depends on the *sign* of the nutation frequency, which is a representation of the spin-locking phase, *i.e.*, whether spin-locking is along  $x$  or  $-x$ . Since the sign of the interaction is opposite for the two cases, the choice determines the sign of  $|S_0\rangle\langle S_0|$  relative to the triplet states, as well as whether the singlet order is transferred back to the  $x$  or  $-x$  direction. Second, since this is a coherent interaction, the amount of magnetization converted to singlet order can be controlled by the length of spin-locking, allowing small portions of magnetization to be utilized at a time, much like a low flip angle pulse. Therefore, SLIC allows the equivalent of rotation direction and flip angle to be controlled as for any classical NMR pulse.

The SLIC sequence can be used to measure  $J$ -coupling and chemical shift differences in nearly-equivalent spin pairs. Figure 8.2 shows measurements of the phenylalanine-glycine-glycine tripeptide molecule.<sup>3</sup>  $J$ -coupling is

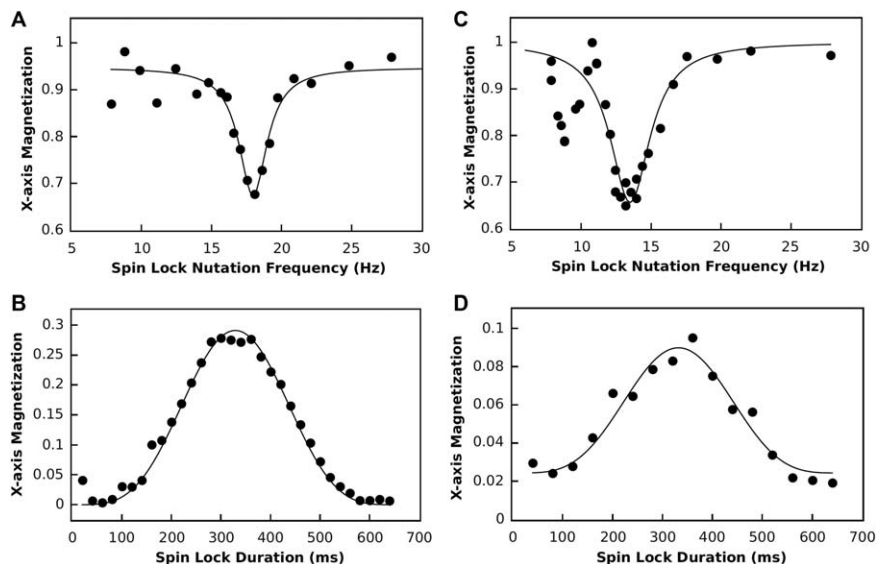


**Figure 8.2** Measurements of  $J$ -couplings and chemical shift differences of two nearly-equivalent spin pairs in the phenylalanine-glycine-glycine tripeptide using the SLIC sequence. Results for the proton pair at  $\delta = 3.71$  ppm: (a) The NMR signal following the first spin-lock pulse as a function of nutation frequency with fixed  $\tau_{SL}$  of 300 ms. The dip occurs when nutation frequency equals  $J$ -coupling and  $x$ -axis magnetization is converted into undetectable singlet order. In this case  $J = 17.5 \pm 0.3$  Hz. (b) The NMR signal following the full SLIC experiment as a function of spin-lock duration  $\tau_{SL}$ , with  $\tau_{evolve} = 5$  s. The maximum occurs when  $\tau_{SL} = 1/(\Delta\nu\sqrt{2})$ . Here  $\Delta\nu = 2.15 \pm 0.02$  Hz was measured. Results for the proton pair at  $\delta = 3.20$  ppm: (c and d) For the second spin pair, the same procedure measured  $J = 13.5 \pm 0.2$  Hz and  $\Delta\nu = 2.13 \pm 0.06$  Hz. Reproduced from ref. 3 with permission from American Physical Society, Copyright 2013.

measured by performing either the full SLIC sequence or half sequence (acquiring the spectrum after the first SLIC pulse) as a function of nutation frequency. If the half sequence is used, a Lorentzian-shaped dip occurs at the  $J$ -coupling frequency. Chemical shift difference can also be measured with either sequence by plotting intensity as a function of spin-locking duration  $\tau_{SL}$ . Using the full sequence results in an intensity curve following the function  $I = A \sin^4(\pi\tau_{SL}\Delta\nu/\sqrt{2})$ .

There are both benefits and drawbacks to using SLIC *versus* M2S. One benefit is much lower specific absorption rate (SAR) with SLIC,<sup>28</sup> since the power absorbed by a sample is proportional to the square of  $B_1$ . Another is that SLIC begins converting  $x$ -axis magnetization to the long-lived singlet state immediately, whereas M2S goes through an intermediate coherence with a shorter lifetime.<sup>3</sup> The sequences have the same transfer efficiency in the absence of relaxation; however, in the presence of relaxation SLIC can be

more efficient, particularly if  $T_1$  is short. SLIC has a relatively narrow bandwidth for  $B_1$  and  $B_0$  offsets in which it will work, and the longer the SLIC pulse is applied, the narrower the bandwidth gets, which can be problematic for very small  $\Delta\nu$ . The composite  $180^\circ$  pulses of M2S are resistant to  $B_1$  offsets, but the sequence is still sensitive to  $B_0$  offset.<sup>3</sup> Some of these issues can be ameliorated using adiabatic SLIC pulses,<sup>28–31</sup> discussed at the end of the chapter. On the other hand, the narrow bandwidth of SLIC can enable the selective creation of singlet states on one pair of spins when many pairs are present.<sup>23</sup> Finally, it can be difficult to create properly shaped weak spin-locking pulses due to hardware issues such as passive transmit-receive switches, which may require a minimum turn-on voltage that is comparable to the RF magnitude.

### 8.3 Four-spin Systems

In a four-spin configuration, singlet states can exist on different pairs of spins depending on the geometry, couplings and chemical shifts of the spin system. Four identical spins have two singlet, three triplet and one quadruplet state, but this is an uncommon situation that has not been explored. More commonly, the system has two separate pairs of equivalent or nearly-equivalent spins (an AA'BB' system), with either a strongly coupled inner pair and a weakly coupled outer pair (Figure 8.3b,  $J_{AA'} > J_{AB} > J_{BB'}$ ), or two strongly coupled pairs with weak inter-pair coupling (Figure 8.3c,  $J_{AA'}$  and  $J_{BB'} \gg J_{AB}$ ,  $\Delta\nu_{AA'}$ , and  $\Delta\nu_{BB'}$ ). The first situation is typically found in  $^{13}\text{C}$ -labelled alkenes and is important for para-hydrogen induced polarization techniques. It can also be found in some aromatic systems. The second is common in polypeptides and alkanes. From a quantum mechanical standpoint, the mathematics is the same for both cases. However, they will be analyzed separately because the energy difference between  $^{13}\text{C}$  and protons that is common in the first geometry leads to different results from the all-proton case common in the second.

In all cases the model Hamiltonian includes six  $J$ -couplings among the four spins. Again, only liquid and gas systems are considered so that dipolar coupling can be ignored. The coupling Hamiltonian is:

$$\hat{\mathcal{H}}_J = J_{AA'} \hat{\mathbf{I}}_A \cdot \hat{\mathbf{I}}_{A'} + J_{BB'} \hat{\mathbf{I}}_B \cdot \hat{\mathbf{I}}_{B'} + J_{AB} \hat{\mathbf{I}}_A \cdot \hat{\mathbf{I}}_B + J_{A'B'} \hat{\mathbf{I}}_{A'} \cdot \hat{\mathbf{I}}_{B'} + J_{AB'} \hat{\mathbf{I}}_A \cdot \hat{\mathbf{I}}_{B'} + J_{A'B} \hat{\mathbf{I}}_{A'} \cdot \hat{\mathbf{I}}_B \quad (8.8)$$

For the cases where the pairs are different nuclear species, such a pair of  $^{13}\text{C}$  with a pair of protons, one can make the secular approximation, but there is no difference in the results compared with using the full Hamiltonian.

Diagonalization proceeds as in the two-spin case, but this time using product states of singlets and triplets taken from the two separate pairs. These can be divided into symmetric and anti-symmetric combinations, which can be analyzed separately. Manipulation of the symmetric combinations  $SS$  and  $TT$  enables simultaneous creation of singlet order on two pairs

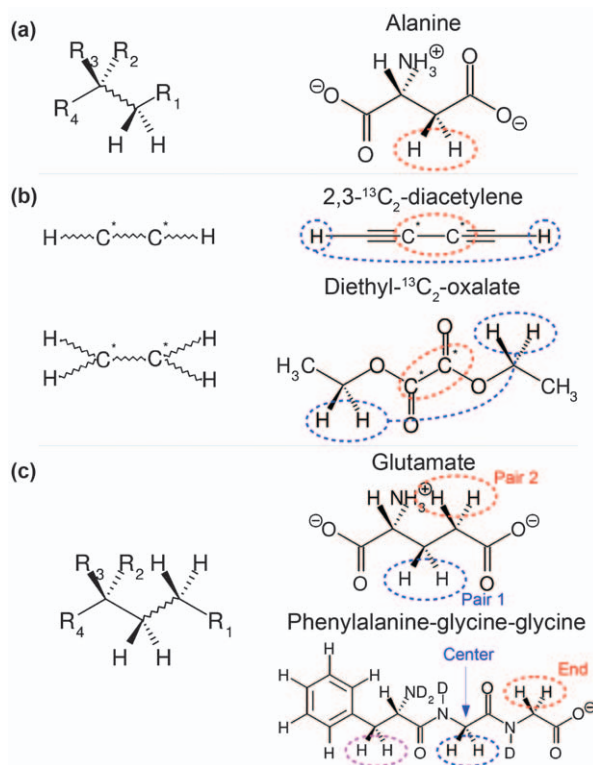


**Figure 8.3** Example families of molecular structures used for singlet state experiments. Squiggly lines indicate that a variable number of intervening geminal protons is possible. (a) A pair of inequivalent or nearly equivalent geminal protons. Examples: aspartate, citric acid, glycerol formal. (b) One pair of identical spins sandwiched between one or more pairs of identical spins of a different nucleus (here \* indicates locations enriched with  $^{13}\text{C}$ ). Examples: diacetylene, diethyloxalate. (c) Two or more pairs of nearly equivalent protons. Examples: glutamate, phenylalanine-glycine-glycine. Other geometries not shown include vicinal proton pairs, neighboring  $^{15}\text{N}$  nuclei and neighboring phosphate groups. Reproduced from ref. 23 with permission from Elsevier, Copyright 2016.

of equivalent spins, while manipulation of anti-symmetric combinations  $ST$  and  $TS$  enables the population of individual singlet states as well as transfer of singlet order between different spin pairs.

First consider the case where an inner pair  $B$  is far off-resonance from an outer pair  $A$  (for example  $A$  are protons and  $B$  are  $^{13}\text{C}$ ). In this case spin-locking can be applied to either pair  $A$  or  $B$  independently with nutation frequency  $\nu_n$ . If spin-locking is only applied to  $A$  (the protons in our example), the relevant singlet and triplet states are  $|S_{0A}\rangle$ ,  $|S_{0B}\rangle$ ,  $|\phi_{-A}\rangle$ ,  $|\phi_{+A}\rangle$ ,  $|\phi_{0A}\rangle$ ,  $|T_{-B}\rangle$ ,  $|T_{+B}\rangle$ , and  $|T_{0B}\rangle$ . The spin-locked triplet states are used for  $A$ , and the bare triplet states are used for  $B$ . Consider first the

Hamiltonian for symmetric product states  $|S_{0A}S_{0B}\rangle$ ,  $|\phi_{-A}T_{0B}\rangle$ ,  $|\phi_{0A}T_{0B}\rangle$ ,  $|\phi_{+A}T_{0B}\rangle$ :

$$\hat{\mathcal{H}} = \begin{bmatrix} -(J_{AA'} + J_{BB'}) & \frac{J_{AB} + J_{A'B'} - J_{AB'} - J_{A'B}}{4\sqrt{2}} & 0 & \frac{J_{AB'} + J_{A'B} - J_{AB} - J_{A'B'}}{4\sqrt{2}} \\ \frac{J_{AB} + J_{A'B'} - J_{AB'} - J_{A'B}}{4\sqrt{2}} & v_n & 0 & 0 \\ 0 & 0 & 0 & 0 \\ \frac{J_{AB'} + J_{A'B} - J_{AB} - J_{A'B'}}{4\sqrt{2}} & 0 & 0 & -v_n \end{bmatrix}. \quad (8.9)$$

The Hamiltonian is very similar to the two-spin system, but with energy levels of the product singlet state now determined by the sum of  $J$ -couplings for the individual singlet states, and with the coherent interaction now driven by a  $J$ -coupling difference rather than a chemical shift difference. The crossing occurs when  $v_n = \pm (J_{AA'} + J_{BB'})$ . In this case, magnetization from the triplet states of both spin pairs is simultaneously converted to singlet order in both spin pairs. Significantly, because spin-locking only needs to be applied to one of the two sets of spins, a  $^{13}\text{C}$  singlet can be populated and read out using equipment only designed for protons, significantly increasing the utility of this approach.

This method has been used to populate singlet states in symmetric molecules that have a pair of equivalent  $^{13}\text{C}$  or  $^{15}\text{N}$  spins.<sup>32,33</sup> Similar results can be achieved even when there are four or six outer spins, or when the outer spins are spin-1 such as deuterium, as long as they are all magnetically equivalent.<sup>34,35</sup> Following para-hydrogen induced polarization *via* hydrogenation or signal amplification by reversible exchange (SABRE), SLIC is a very useful method for transferring singlet order to triplet magnetization for readout, and it eliminates the need to create a level crossing *via* field cycling.<sup>11–22</sup> Techniques utilizing this approach include SLIC-SABRE, LIGHT-SABRE, DARTH-SABRE and QUASR-SABRE.

For the anti-symmetric product states  $|S_{0A}T_{0B}\rangle$ ,  $|\phi_{-A}S_{0B}\rangle$ ,  $|\phi_{0A}S_{0B}\rangle$ ,  $|\phi_{+A}S_{0B}\rangle$ , the Hamiltonian is

$$\hat{\mathcal{H}} = \begin{bmatrix} -(J_{AA'} - J_{BB'}) & \frac{J_{AB} + J_{A'B'} - J_{AB'} - J_{A'B}}{4\sqrt{2}} & 0 & \frac{J_{AB'} + J_{A'B} - J_{AB} - J_{A'B'}}{4\sqrt{2}} \\ \frac{J_{AB} + J_{A'B'} - J_{AB'} - J_{A'B}}{4\sqrt{2}} & v_n & 0 & 0 \\ 0 & 0 & 0 & 0 \\ \frac{J_{AB'} + J_{A'B} - J_{AB} - J_{A'B'}}{4\sqrt{2}} & 0 & 0 & -v_n \end{bmatrix}. \quad (8.10)$$

Again, spin-locking with nutation frequency  $\nu_n$  can be applied to either spin pair independently, and in this example it has been applied to spin pair A. Now the crossing occurs when the nutation frequency equals the difference in intra-pair  $J$ -couplings rather than the sum. Singlet order is created on whichever spin pair is irradiated, while it is depleted on the other. Since initially only triplet states are typically populated, only half as much singlet order is created, and the signal strength is lower than in the  $TT \rightarrow SS$  case. However, if one of the singlet states is already populated, its singlet order is transferred to the other. In the context of para-hydrogen induced polarization, this may be very useful for transferring singlet order from the protons to a pair of  $^{13}\text{C}$  or  $^{15}\text{N}$ , which can have a very long singlet lifetime.

Note that it is also possible to find molecules of a similar geometry with two pairs of protons, or with a pair of protons and a pair of methylene groups.<sup>36</sup> Depending on spin-locking power and chemical shifts, both spins may then experience spin-locking, and the  $|\phi\rangle$  triplet states would need to be used for both pairs. In that case the following analysis below is the appropriate one.

For the second geometry, assume there are two spin pairs A and B, such that  $J_{AA'}$  and  $J_{BB'}$  are much greater than  $J_{AB}$ ,  $J_{AB'}$ ,  $J_{A'B}$  and  $J_{A'B'}$ . An example is two pairs of protons separated by a few bonds in a chain, such as in a polypeptide.<sup>23</sup> The proton chemical shifts are similar enough that both pairs are spin-locked at the same time. Again, there are 16 product states, but this time spin-locked triplet states must be used for both pairs. One can show that in this case there is an interaction  $C$  where

$$C = \langle \phi_{0A} S_{0B} | \hat{\mathcal{H}}_J | S_{0A} \phi_{0B} \rangle = \langle \phi_{+A} S_{0B} | \hat{\mathcal{H}}_J | S_{0A} \phi_{+B} \rangle = \langle \phi_{-A} S_{0B} | \hat{\mathcal{H}}_J | S_{0A} \phi_{-B} \rangle$$

$$= \frac{J_{AB} + J_{A'B'} - J_{AB'} - J_{A'B}}{4}. \quad (8.11)$$

This is similar to the results from eqn (8.10), but with a different denominator due to the second pair having  $|\phi\rangle$  instead of  $|T\rangle$  eigenstates. Also, there is now an interaction between  $|S_0\phi_0\rangle$  and  $|\phi_0S_0\rangle$ , but these states do not change energy with spin-locking and cannot be brought on resonance. For this geometry, the interaction term represents an average difference between  $J$ -couplings on the same side of the bond *vs.* opposite side (*syn vs. anti*), which in most molecules is small but non-zero. There is also a family of interactions driven by the difference between  $J$ -couplings on one side *vs.* those on the other, such as

$$\langle \phi_{0A} \phi_{-B} | H_J | \phi_{-A} S_{0B} \rangle = \frac{J_{AB} - J_{A'B'} - J_{AB'} + J_{A'B}}{4}. \quad (8.12)$$

These connect triplet-triplet combinations with triplet-singlet combinations, but the interaction term is generally much smaller than in eqn (8.11).

Two Hamiltonians of two-level systems can be written, for the triplet-singlet product states  $|S_0\phi_-\rangle$  and  $|\phi_-S_0\rangle$  as well as for  $|S_0\phi_+\rangle$  and  $|\phi_+S_0\rangle$ :

$$\begin{aligned}\hat{\mathcal{H}}_1 &= \begin{bmatrix} J_{AA'} - J_{BB'} & C \\ C & \nu_{n,B} - \nu_{n,A} \end{bmatrix}, \\ \hat{\mathcal{H}}_2 &= \begin{bmatrix} J_{AA'} - J_{BB'} & C \\ C & \nu_{n,A} - \nu_{n,B} \end{bmatrix}.\end{aligned}\quad (8.13)$$

The general condition for a crossing to occur is  $|\Delta\nu_n| = |\nu_{n,A} - \nu_{n,B}| = |J_{AA'} - J_{BB'}|$ , where  $\nu_{n,A}$  and  $\nu_{n,B}$  are the effective nutation frequencies for spin pairs  $A$  and  $B$ . If spin-locking is applied on resonance with spin pair  $A$ , and the resonance frequency difference between spin pairs  $A$  and  $B$  is  $\Delta\nu_{AB}$ , then

$$\Delta\nu_n = \sqrt{\nu_{n,A}^2 + \Delta\nu_{AB}^2} - \nu_{n,A}.$$

Given a particular resonance frequency difference, a nutation frequency difference can be chosen so that the singlet-triplet product states are on resonance and singlet order will be coherently driven from one spin pair to the other. Typical chemical shift values allow this condition to be met while applying relatively strong spin-locking. Consequently, even spin pairs with  $\Delta\nu > J_{12}$  can be used, since their eigenstates will be converted to singlet and triplets upon spin-locking.

Note that only a subset of singlet-triplet product states can participate, those whose partner spin pair are in the correct triplet state for a given sign of nutation frequency (*i.e.*, direction of  $B_1$ ). In this case the singlet state should become entangled with the appropriate triplet state. However, if the triplet states interchange quickly enough and remain in equilibrium during the interactions, then the interaction will appear to be independent of spin-locking direction, and the triplet states play a purely ancillary role by bringing the energy levels into resonance.

Figure 8.4 shows an example of singlet state transfer between two spin pairs in glutamate.<sup>23</sup> Singlet order was prepared on one spin pair and read out from either the same pair or the other following a period of spin-locking, resulting in a sinusoidal signal when plotted as a function of spin-lock duration. The experiment was also performed in phenylalanine-glycine-glycine, where the long lifetimes of the singlet states enabled the measurement of a very small coupling difference,  $|J_{\text{syn}} - J_{\text{anti}}| = \sim 8$  mHz.

## 8.4 Other Spin Systems

SLIC sequences have also been used to convert singlet order in a proton pair to magnetization in a single nearby  $^{13}\text{C}$  nucleus.<sup>36</sup> The eight product states are given by the singlet and triplet states from the protons multiplied with  $|\uparrow\rangle$  or  $|\downarrow\rangle$ , the Zeeman states of  $^{13}\text{C}$ . When spin-locking only the protons with a

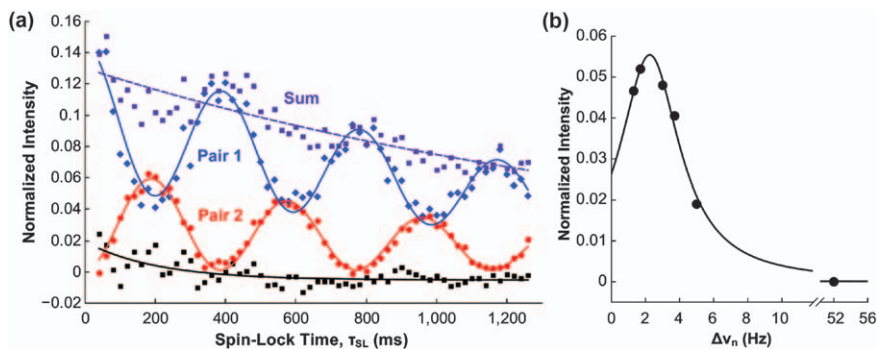


**Figure 8.4** Measurement of coherent singlet state transfer between spin pairs in glutamate. (a) Singlet order is selectively prepared predominantly in spin pair 1 and is followed with spin-locking at a 500 Hz nutation rate during the evolution time. The singlet state is then read out from either spin pair 1 (blue points) or spin pair 2 (red points). Oscillations in the singlet state population of each spin pair indicate  $|J_{\text{syn}} - J_{\text{anti}}| = 2.57 \pm 0.04$  Hz. If spin-locking is not applied, singlet transfer does not occur (black points). (b) The amplitude of singlet transfer is plotted for singlet transfer measurements performed with a range of spin-locking nutation frequencies. A Lorentzian fit gives a peak value of  $2.25 \pm 0.08$  Hz for the resonance condition with a full-width half-maximum bandwidth of  $4.3 \pm 0.4$  Hz. Reproduced from ref. 23 with permission from Elsevier, Copyright 2016.

nutation frequency  $\nu_n = J_{AB}$  (the  $J$ -coupling between protons),  $|S_0 \uparrow\rangle$  and  $|S_0 \downarrow\rangle$  cross with  $|\phi_+ \downarrow\rangle$  and  $|\phi_+ \uparrow\rangle$ , respectively, all with interaction term  $(J_{AX} - J_{BX})/4\sqrt{2}$ . Proton magnetization is converted to proton singlet order while the  $^{13}\text{C}$  population is inverted, but there is no polarization transfer to  $^{13}\text{C}$ . In this case, the differential coupling with  $^{13}\text{C}$  rather than chemical shift difference produces magnetic inequivalence in the protons and drives the conversion. Spin-locking only  $^{13}\text{C}$  with the same nutation frequency produces a crossing between  $|S_0 \uparrow_x\rangle$  and both  $|T_- \downarrow_x\rangle$  and  $|T_+ \downarrow_x\rangle$  (where  $|\downarrow_x\rangle$  and  $|\uparrow_x\rangle$  are the Zeeman states rotated along the spin-locked axis). It therefore creates transverse  $^{13}\text{C}$  magnetization along the spin-locking direction proportional to the level of proton singlet order. This is similar to Hartmann–Hahn polarization transfer, but the  $^{13}\text{C}$  spin-locking nutation frequency is now matched to the singlet–triplet energy difference of the proton system. The method was successfully used to produce 9% polarization on a  $^{13}\text{C}$  nucleus in an 11.7 T magnet following para-hydrogen addition.<sup>37</sup>

In situations with many strongly coupled spins, the eigenstates are mixed into more complex states defined by angular momentum quantum numbers  $F$  and  $m_F$  determined by molecular geometry and couplings. In one example, propane was hyperpolarized with para-hydrogen and SLIC was used to transfer singlet order to observable magnetization.<sup>13</sup> The transfer was performed at a low magnetic field (0.05 T) so that all protons were strongly coupled, which resulted in four crossings between the hyperpolarized and observable states occurring at integer multiples of  $J$  (Figure 8.5). Similar crossings have been measured in ethanol.<sup>38</sup>

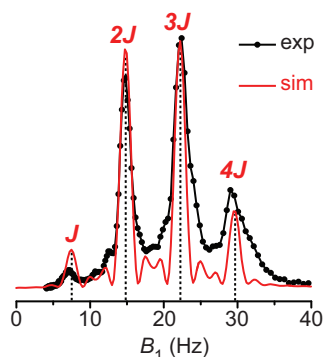


**Figure 8.5** Experimentally measured (black circles and trace) and theoretically calculated (red trace) dependence of the SLIC induced hyperpolarized propane signal on  $B_1$  amplitude with SLIC pulse duration  $\tau_{SL} = 0.5$  s. Reproduced from ref. 13 with permission from Elsevier, Copyright 2017.

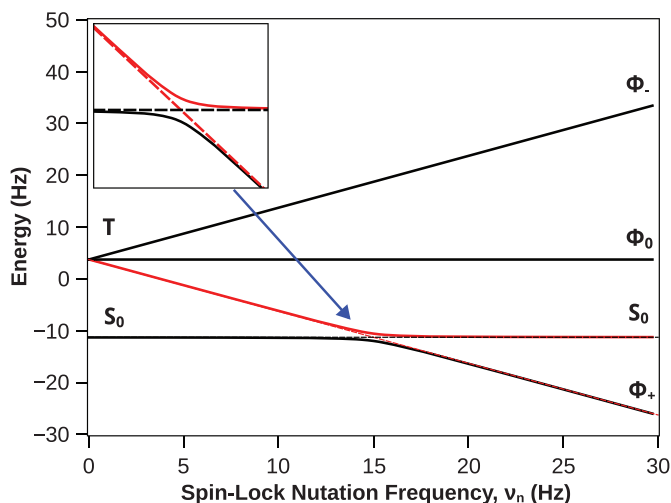
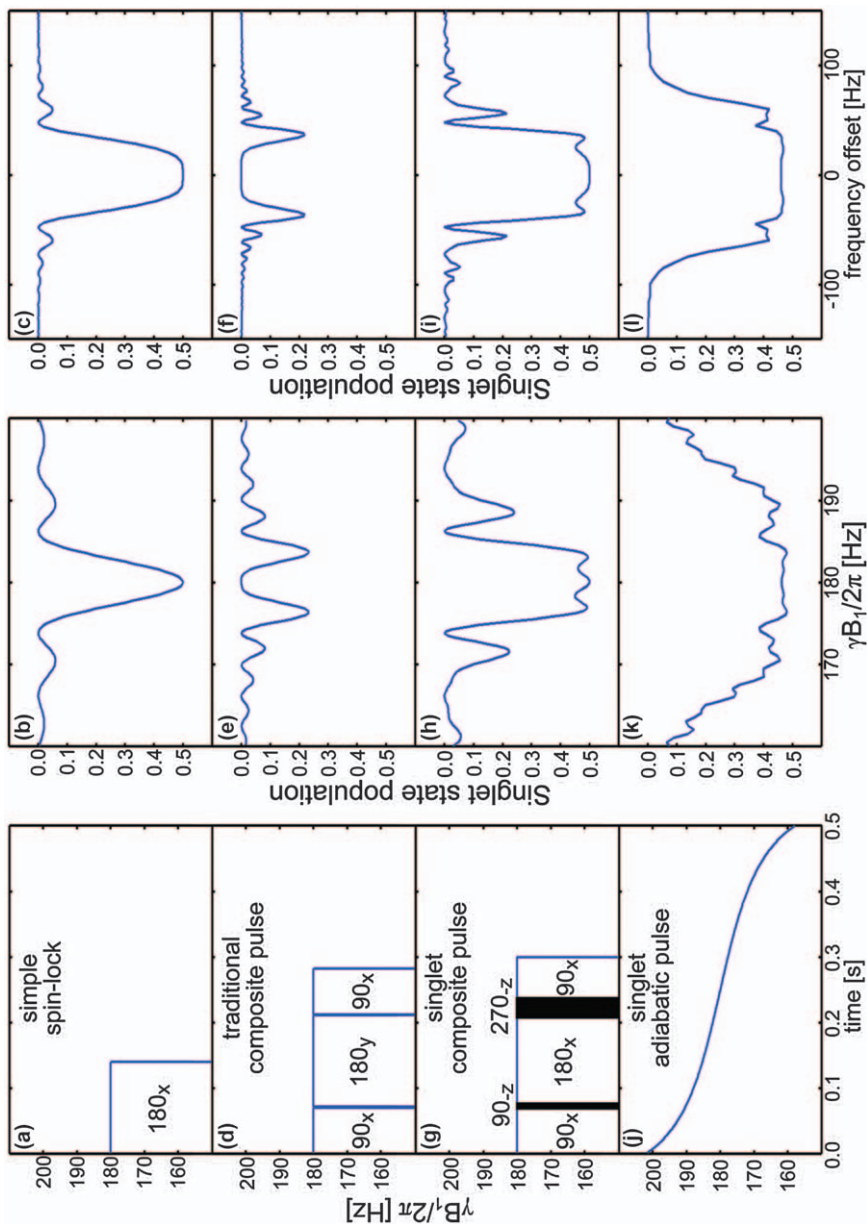


**Figure 8.6** Energy levels of triplet and singlet states for a two spin-1/2 system with  $J$ -coupling of 15 Hz and chemical shift difference of 2 Hz. Solid lines represent the energy levels following diagonalization of eqn (8.7). Following a  $90^\circ$  pulse, if the spin-locking strength is gradually increased through the SLIC resonance condition slowly enough, magnetization follows the solid red pathway resulting in singlet order. If  $B_1$  is instead switched on suddenly, as in a hard pulse, magnetization follows the dashed red pathway and remains in the triplet state. The inset shows an expanded view of the avoided crossing.

## 8.5 Adiabatic SLIC

Diagonalization of the full Hamiltonian given by eqn (8.7) or (8.9) would show energy levels with an avoided crossing at their resonance conditions ( $\pm\nu_n = J$  or  $\pm\nu_n = J_{AA'} + J_{BB'}$ , respectively, see Figure 8.6). If the nutation



frequency is slowly swept through the anti-crossing, adiabatic population transfer occurs between triplet and singlet states.<sup>28,30,31,39</sup> This method has the advantage of a broader  $B_1$  and  $B_0$  bandwidth, which is particularly useful if  $J$  is not well known or if there are  $B_1$  or  $B_0$  inhomogeneities (Figure 8.7). An adiabatic pulse can be used in place of any of the CW SLIC pulses previously discussed. Another alternative, called adiabatic-passage spin order conversion (APSOC), uses a single adiabatic ramped pulse through  $\nu_n = J$  with the resonance frequency set at an appropriate offset.<sup>29</sup> In this case, the initial  $90^\circ$  pulse can be done away with, and longitudinal magnetization is converted directly to singlet order and *vice versa*. APSOC has the advantage of working even for systems of spins far from equivalence ( $\Delta\nu > J$ ) that must be spin-locked for preservation.

## 8.6 Conclusion and Outlook

Spin-lock induced crossing and related sequences can be used as an alternative to hard pulse sequences for singlet order creation and manipulation. In addition to the situations referenced above, they have been utilized for diverse measurements in  $^1\text{H}$  and  $^{13}\text{C}$  spin pairs, monodeuterated methyl groups, photo-PHIP and dendrimers.<sup>40–46</sup> Compared with hard-pulse sequences, SLIC sequences can enable more selective control of the spin system with much smaller power deposition in samples, at the expense of more stringent requirements for  $B_1$  and  $B_0$ . Their low SAR is particularly attractive for applications in humans and animals, where estimates of SAR for hard pulse sequences is at or above most safety limits.

The methods outlined here are quite general and can be applied even to spin systems with eigenstates other than singlets and triplets. There are many situations where they have yet to be fully explored, for example in solid systems with strong dipolar coupling,<sup>47</sup> at low fields where all spins are strongly coupled and for electron paramagnetic resonance.<sup>48</sup> Moreover, since spin-locking is analogous to the AC Stark effect (or Autler–Townes effect) for electric fields,<sup>27,49</sup> numerous phenomena observed in optical systems under the influence of driving fields may also be possible to replicate with nuclear spins in organic molecules.

**Figure 8.7** Simulations of singlet order creation using a variety of SLIC pulse shapes. (a–c) A simple SLIC pulse with 5 Hz bandwidth in  $B_1$  amplitude and 62 Hz bandwidth in RF offset. (d–f) A traditional composite pulse, which fails to produce singlet state. (g–i) A modified composite pulse for creating singlet order, with bandwidth of 10 Hz in  $B_1$  amplitude and 84 Hz in RF offset. (j–l) An adiabatic SLIC pulse with a tangent  $B_1$  amplitude sweep providing a bandwidth of 30 Hz in  $B_1$  amplitude and 140 Hz in RF offset.

Reproduced from ref. 28 with permission from AIP Publishing.

## References

1. M. H. Levitt, *Spin Dynamics*, John Wiley & Sons, Ltd., West Sussex, England, 2nd edn, **vol. 12**, 2008, pp. 305–306.
2. S. J. DeVience, R. L. Walsworth and M. S. Rosen, *J. Magn. Reson.*, 2012, **218**, 5.
3. S. J. DeVience, R. L. Walsworth and M. S. Rosen, *Phys. Rev. Lett.*, 2013, **111**, 173002.
4. G. Pileio, J.-N. Dumez, I.-A. Pop, J. T. Hill-Cousins and R. C. D. Brown, *J. Magn. Reson.*, 2015, **252**, 130–134.
5. M. C. D. Tayler, I. Marco-Rius, M. I. Kettunen, K. M. Brindle, M. H. Levitt and G. Pileio, *J. Am. Chem. Soc.*, 2012, **134**, 7668–7671.
6. J.-N. Dumez, B. Vuichoud, D. Mammoli, A. Bornet, A. C. Pinon, G. Stevanato, B. Meier, G. Bodenhausen, S. Jannin and M. H. Levitt, *J. Phys. Chem. Lett.*, 2017, **8**, 3549–3555.
7. W. S. Warren, E. Jenista, R. T. Branca and X. Chen, *Science*, 2009, **323**, 1711–1714.
8. P. R. Vasos, A. Comment, R. Sarkar, P. Ahuja, S. Jannin, J.-P. Ansermet, J. A. Konter, P. Hautle, B. van den Brandt and G. Bodenhausen, *Proc. Nat. Acad. Sci. U.S.A.*, 2009, **106**, 18469–18473.
9. P. Ahuja, R. Sarkar, S. Jannin, P. R. Vasos and G. Bodenhausen, *Chem. Commun.*, 2010, **46**, 8192–8194.
10. G. Pileio, S. Bowen, C. Laustsen, M. C. D. Tayler, J. T. Hill-Cousins, L. J. Brown, R. C. D. Brown, J. H. Ardenkjaer-Larsen and M. H. Levitt, *J. Am. Chem. Soc.*, 2013, **135**, 5084–5088.
11. D. A. Barskiy, O. G. Salnikov, R. V. Shchepin, M. A. Feldman, A. M. Coffey, K. V. Kovtunov, I. V. Koptyug and E. Y. Chekmenev, *J. Phys. Chem. C*, 2016, **120**, 29098.
12. D. V. Kovtunov, M. L. Truong, D. A. Barskiy, I. V. Koptyug, A. M. Coffey, K. W. Waddell and E. Y. Chekmenev, *Chem. Eur. J.*, 2014, **20**, 14629.
13. D. A. Barskiy, O. G. Salnikov, A. S. Romanov, M. A. Feldman, A. M. Coffey, K. V. Kovtunov, I. V. Koptyug and E. Y. Chekmenev, *J. Magn. Reson.*, 2017, **276**, 78.
14. T. Theis, M. Truong, A. M. Coffey, E. Y. Chekmenev and W. S. Warren, *J. Magn. Reson.*, 2014, **248**, 23.
15. J. R. Lindale, S. L. Eriksson, C. P. N. Tanner, Z. Zhou, J. F. P. Colell, G. Zhang, J. Bae, E. Y. Chekmenev, T. Theis and W. S. Warren, *Nat. Commun.*, 2019, **10**, 395.
16. S. Knecht, A. S. Kiryutin, A. V. Yurkovskaya and K. L. Ivanov, arXiv: 1802.04471.
17. A. N. Pravdivtsev, A. V. Yurkovskaya, N. N. Lukzen, H.-M. Vieth and K. L. Ivanov, *Phys. Chem. Chem. Phys.*, 2014, **16**, 18707.
18. A. N. Pravdivtsev, A. V. Yurkovskaya, N. N. Lukzen, K. L. Ivanov and H.-M. Vieth, *J. Phys. Chem. Lett.*, 2014, **5**, 3421.

19. A. N. Pravdivtsev, I. V. Skovpin, A. I. Svyatova, N. V. Chukanov, L. M. Kovtunova, V. I. Bukhtiyarov, E. Y. Chekmenev, K. V. Kovtunov, I. V. Koptyug and J.-B. Hövener, *J. Phys. Chem. A*, 2018, **122**, 9107.
20. T. Theis, N. M. Ariyasingha, R. V. Shchepin, J. R. Lindale, W. S. Warren and E. Y. Chekmenev, *J. Phys. Chem. Lett.*, 2018, **9**, 6136.
21. A. S. Kiryutin, H. Zimmerman, A. V. Yurkovskaya, H.-M. Vieth and K. L. Ivanov, *J. Magn. Reson.*, 2015, **261**, 64.
22. V. V. Zhivonitko, J. Bresien, A. Schulz and I. V. Koptyug, *Phys. Chem. Chem. Phys.*, 2019, **21**, 5890–5893.
23. S. J. DeVience, R. L. Walsworth and M. S. Rosen, *J. Magn. Reson.*, 2016, **262**, 42.
24. M. H. Levitt, *Spin Dynamics*, John Wiley & Sons, Ltd., West Sussex, England, 2nd edn, **vol. 14**, 2008, pp. 359–360.
25. G. Pileio, *Prog. Nucl. Magn. Reson. Spectrosc.*, 2016, **98–99**, 1.
26. G. Pileio, M. Carravetta and M. H. Levitt, *Proc. Natl. Acad. Sci. U. S. A.*, 2010, **107**, 17135.
27. M. C. D. Tayler and M. H. Levitt, *Phys. Chem. Chem. Phys.*, 2011, **13**, 5556.
28. T. Theis, Y. Feng, T. Wu and W. S. Warren, *J. Chem. Phys.*, 2014, **140**, 014201.
29. A. N. Pravdivtsev, A. S. Kiryutin, A. V. Yurkovskaya, H.-M. Vieth and K. L. Ivanov, *J. Magn. Reson.*, 2016, **273**, 56.
30. B. A. Rodin, A. S. Kiryutin, A. V. Yurkovskaya, K. L. Ivanov, S. Yamamoto, K. Sato and T. Takui, *J. Magn. Reson.*, 2018, **291**, 14.
31. B. A. Rodin, K. F. Sheberstov, A. S. Kiryutin, J. T. Hill-Cousins, L. J. Brown, R. C. D. Brown, B. Jamain, H. Zimmermann, R. Z. Sagdeev, A. V. Yurkovskaya and K. L. Ivanov, *J. Chem. Phys.*, 2019, **150**, 064201.
32. K. Claytor, T. Theis, Y. Feng and W. Warren, *J. Magn. Reson.*, 2014, **239**, 81.
33. K. F. Sheberstov, H.-M. Vieth, H. Zimmermann, K. L. Ivanov, A. S. Kiryutin and A. V. Yurkovskaya, *Appl. Magn. Reson.*, 2018, **49**, 293.
34. Y. Feng, T. Theis, T. Wu, K. Claytor and W. S. Warren, *J. Chem. Phys.*, 2014, **141**, 134307.
35. K. Claytor, T. Theis, Y. Feng, J. Yu, D. Gooden and W. S. Warren, *J. Am. Chem. Soc.*, 2014, **136**, 15118.
36. Y. Zhang, K. Basu, J. W. Canary and A. Jerschow, *Phys. Chem. Chem. Phys.*, 2015, **37**, 24370.
37. J. Eills, G. Stevanato, C. Bengs, S. Glöggler, S. J. Elliot, J. Alonso-Valdesueiro, G. Pileio and M. H. Levitt, *J. Magn. Reson.*, 2017, **274**, 163.
38. S. J. DeVience, PhD thesis, Harvard University, 2014.
39. B. Kharkov, X. Duan, J. W. Canary and A. Jerschow, *J. Magn. Reson.*, 2017, **284**, 1.
40. Y. Zhang, P. C. Soon, A. Jerschow and J. W. Canary, *Angew. Chem., Int. Ed.*, 2014, **53**, 3396.
41. Y. Zhang, K. Basu, J. W. Canary and A. Jerschow, *Phys. Chem. Chem. Phys.*, 2015, **17**, 24370.

42. S. J. Elliott, L. J. Brown, J.-N. Dumez and M. H. Levitt, *Phys. Chem. Chem. Phys.*, 2016, **18**, 17965.
43. S. J. Elliott, L. J. Brown, J.-N. Dumez and M. H. Levitt, *J. Magn. Reson.*, 2016, **272**, 87.
44. O. M. Ogba, S. J. Elliott, D. A. Kolin, L. J. Brown, S. Cevalios, S. Sawyer, M. H. Levitt and D. J. O'Leary, *J. Org. Chem.*, 2017, **82**, 8943.
45. A. N. Pravdivtsev, A. V. Yurkovskaya, P. A. Petrov and H.-M. Vieth, *Phys. Chem. Chem. Phys.*, 2017, **19**, 25961.
46. P. Saul, S. Mamone and S. Glöggler, *Chem. Sci.*, 2019, **10**, 413–417.
47. Q. Chen, I. Schwarz and M. B. Plenio, *Phys. Rev. B*, 2017, **95**, 224105.
48. K. L. Ivanov and N. N. Lukzen, *Mol. Phys.*, 2019, DOI: 10.1080/00268976.2018.1562121.
49. J. S. Bakos, *Phys. Rep.*, 1977, **31**, 209.